3D-MGNet: Integrating Radiomics and Deep Learning for Enhanced Meningioma Grading

Zhuo Zhang*, Yihan Wen*, Peiyu Wang, Ying Miao, *and* Guanchong Niu

***Abstract*—Meningiomas are among the most common primary intracranial tumors in adults, exhibiting varying biological behaviors across different grades. High-grade meningiomas display aggressive behavior, and the survival and prognosis of patients largely depend on the treatment strategy. Therefore, preoperative grading for meningiomas holds significant clinical importance. In recent years, computer-aided diagnosis techniques based on radiomics and deep learning methods have achieved notable success due to their non-invasive advantages for preoperative evaluation. However, most studies face limitations due to the singular source of dataset information, resulting in lower accuracy and reliability issues. To solve the above issues, we design a multimodel classification network named 3D-MGNet to significantly enhance the preoperative grading of meningiomas by integrating dual MRI modalities: T1 CE and T2 Flair. The proposed network consists of a Dual Multimodal Meningioma Feature Extractor (DME) designed to leverage the distinct modalities, and a deep-radiomecs features integration discriminator for robust meningiomas grading. A key innovation within our model is the 3D Large Kernel Attention (3D-LKA) mechanism, which efficiently captures global and local characteristics from processes complex, memory-intensive 3D data. This efficiency attributes to the amalgamation of spatial local convolution operations, spatial long-distance convolution operations, and channel convolution operations. Extensive experimentation demonstrates superior performance of the proposed 3D-MGNet in meningioma grading accuracy compared to existing models. .**

***Index Terms*—Meningioma Grading, Deep learning, Multimodal Learning, 3D Large Kernel Attention, Radiomics Feature integration**

I. Introduction

Meningiomas are one of the most common primary intracranial tumors in adults, accounting for approximately 36.7% of all primary brain tumors [1]. According to the World Health Organization (WHO) standards in 2016 [2, 3], meningiomas can be classified into Grade I, Grade II, and Grade III, with each grade displaying different biological behaviors [4–6]. Low-grade meningiomas are classified as Grade I, with their specific pathological subtypes being meningothelial, fibrous, lymphoplasmacyte-rich, angiomatous, transitional, secretory, psammomatous, microcystic, and metaplastic. High-grade meningiomas consists of Grade II and Grade III, with Grade II pathological subtypes being atypical, chordoid, and clear cell types, and Grade III pathological subtypes including anaplastic, rhabdoid, and papillary types [2]. Low-grade meningiomas grow slowly and patients typically have a favorable survival outcome after surgical resection [7]. In contrast, high-grade meningiomas progress rapidly, exhibit invasive behavior, have a higher recurrence rate, and lower survival rate [8–10]. Specifically, the recurrence rate for Grade II meningiomas is 30%-40%, with a 5-year overall survival rate of 78.4%, and for Grade III meningiomas, the recurrence rate is 50%-80%, with a 5-year overall survival rate of 44% [11, 12]. For low-grade meningiomas, clinical treatment usually involves surgery alone. However, for high-grade meningiomas, additional treatment strategies (such as radiotherapy and chemotherapy) are required even after complete resection[5]. Therefore, accurate preoperative grading of meningiomas holds significant clinical importance for treatment decisions.

With the rapid development of medical imaging technologies, non-invasive examination methods have offered greater convenience to patients with meningiomas, especially Magnetic Resonance Imaging (MRI). With its excellent high spatial resolution and soft tissue contrast, MRI provides crucial information for clinicians and aids in guiding treatment decisions[5]. Each MRI modality can provide different types of image information, with T1-Weighted Contrast-Enhanced (T1 CE) and T2 Fluid-Attenuated Inversion Recovery (T2 FLAIR) sequences commonly applied to meningiomas. In T1 CE sequences, meningiomas often appear as distinct enhancement nodules or masses, creating a significant contrast with the surrounding normal tissue. This enhancement effect helps doctors detect and locate meningioma lesions more accurately. On the other hand, the T2 FLAIR sequence uses a special pulse sequence to suppress fluid signals, particularly highlighting edematous areas. In T2 FLAIR sequences, the edematous area around a meningioma typically appears as a high signal. The visualization of these high signal areas aids in assessing the impact of the meningioma on surrounding tissues. Generally, doctors evaluate various characteristics in MRI, such as the shape, size, location, the fuzziness of the tumor's peripheral boundary, and the extent of tumor necrosis [13–16], to assess different grades. However, the interpretation of these features often relies on the knowledge and experience of observer, posing risks of misdiagnosis and inappropri-

This work was supported by the Fundamental Research Funds for the Central Universities of China (20103237888) and Tianjin Research Innovation Project for Postgraduate Students (2022SKY126). *(Zhuo Zhang and Yihan Wen contributed equally to this work) (Corresponding authors: Ying Miao; Guanchong Niu)*

Zhuo Zhang is with the Guangzhou Institute of Technology, Xidian University, Guangzhou, 510555, China, and also with the College of Computer Science, National University of Defense Technology, Changsha, 410073, China (e-mail: 2130070829@tiangong.edu.cn).

Yihan Wen and Guanchong Niu are with the Guangzhou Institute of Technology, Xidian University, Guangzhou, 510555, China (e-mail: wenyihan4396@gmail.com; niuguanchong@xidian.edu.cn).

Peiyu Wang is with the Dalian University of Technology, Dalian, 116000, China (e-mail: qm1919886@mail.dlut.edu.cn).

Ying Miao is with School of Computer Science, Peking University, Beijing, 100871, China (e-mail: miaoyingqfnu@163.com).

ate treatment strategies [17–19]. Additionally, MRI images are typically acquired using sectional scanning technology, meaning that some crucial details may not be observable in a single section, further complicating the manual grading of meningiomas. Therefore, accurate preoperative grading of meningiomas is particularly important.

Computer-aided diagnosis (CAD) is an ideal solution to the challenges of accurate meningioma grading. Among the leading approaches are radiomics and deep learning. Radiomics, as an advanced medical image analysis method, has significant advantages in analyzing tumor heterogeneity [20, 21]. Coupled with machine learning techniques, it can quantify and analyze high-throughput imaging data in detail. Specifically, in meningioma diagnosis, radiomics can extract various features from meningioma images, including shape, edge, and texture features, and then use machine learning classifiers to make non-invasive predictions about meningioma grading and prognosis [22, 23], aiding doctors in making more accurate treatment decisions. Beyond radiomics, deep learning has been extensively applied in medical analysis. Specifically, the designed novel deep neural network models are capable of automatically learning and extracting features from meningioma images. The performance of model is assessed through a loss function, and the backpropagation algorithm guides the update of parameters by calculating gradients, thereby gradually optimizing the model. This end-to-end learning approach effectively capture complex features and relational information, further improving the accuracy of meningioma grading. Deep learning methods have significant advantages in processing medical data. For instance, in the case of meningiomas, deep learning can help doctors better understand the tumor's growth patterns, invasiveness, and prognostic risks, and the performance can be further enhanced through techniques such as transfer learning and data augmentation. Studies have shown that using convolutional neural networks (CNNs) to explore high-level features improves the performance of meningioma grading [24–26]. Moreover, both methods can be combined with multimodal imaging data, such as structural MRI, functional MRI, and electroencephalography, to capture meningioma features from different angles, thereby increasing the accuracy of diagnosis and prognosis predictions. In summary, radiomics and deep learning demonstrate considerable potential and promise in meningioma research, offering more detailed insights into the tumor's intrinsic characteristics to assist doctors in making more accurate and personalized treatment decisions.

In this study, we introduce novel framework integrated by radiomics and deep learning techniques. Specifically, an advanced three-dimensional deep learning network named 3D MGNet is specifically designed for the automated grading of meningiomas. This network leverages a Dual Multimodal Meningioma Feature Extractor (DME) to fully capture the tumor features in T1 CE T2 FLAIR modality, significantly improving the accuracy and automation level of grading. Further, we design a novel 3D-LKA mechanism to process complex, memory-intensive three-dimensional data. This mechanism captures long-range contextual dependencies through large kernel operations [27], integrating the advantages of both global and local attention by leveraging local contextual information, a large receptive field, linear complexity, and dynamic operations. In addition, a new feature enhancement paradigm for meningiomas grading is proposed by seamlessly integrating neural network-extracted deep features with radiomics features to improve the grading accuracy. The designed Deep-radiomics features integration discriminator fuses the high-level semantic information captured by the proposed DME with the detailed, quantitative features extracted from radiomics analysis. The innovative paradigm enables the proposed method achieves a significant improvement in meningioma grading accuracy.

In summary, our contributions are illustrated as follows:

- Development of the 3D MGNet: A specialized three-dimensional deep learning network, named 3D MGNet, is specifically designed for meningioma grading. The network incorporates a Dual Multimodal Meningioma Feature Extractor (DME) to fully exploit the tumor characteristics in T1 CE and T2 FLAIR MRI modalities, thereby significantly improving grading precision.
- Innovative 3D-LKA Mechanism: We introduce a novel 3D Large Kernel Attention (3D-LKA) mechanism to process complex, memory-intensive 3D data efficiently. This mechanism enhances the model's ability to capture long-range contextual dependencies through large kernel operations, integrating both global and local attention features.
- Deep-Radiomics Feature Integration Discriminator: A unique feature enhancement paradigm is proposed by seamlessly integrating neural network-extracted deep features with radiomics features. This approach enriches the model's capability to accurately grade meningiomas by combining high-level semantic information with detailed, quantitative radiomics analysis.

The rest of this paper is organized as follows. Section II describes the related work of meningiomas grading. After that, Section III provides the details on the proposed grading framework, whereas extensive experimental results are presented in Section IV. Finally, the conclusion is given in Section V.

II. Related Work

Medical imaging classification tasks intend to classify and recognize different pathological states or diseases in medical images, such as MRI, CT, or X-rays. Traditional radiology classification primarily relies on doctors judging based on the size of lesions, blood vessel distribution, density, and other information in the images. However, for complex image features, the human eye often struggles to capture, and subjective assessment may overlook important features and details of diseases[28][29], thus limiting the improvement of classification performance. To overcome the challenges in preoperative assessment tasks of tumors and related diseases in traditional medical imaging, imaging omics based on machine learning has become a promising evaluation method. The concept of radiomics was proposed by the Dutch scholar Lambin in 2012[30][31]. It is a method of analyzing and modeling using a large number of quantitative features in medical images. Specifically, radiomics mainly extracts features such as

morphology, texture, and intensity from images, transforming digital medical images containing rich pathological physiological information into exploitable quantitative high-dimensional features, and applies machine learning algorithms (such as Support Vector Machine (SVM), Random Forest (RF), and Linear Discriminant Analysis (LDA), etc.)[32][33][34][35] to achieve non-invasive prediction of disease states, efficacy, prognosis, and other factors[36]. Currently, radiomics has tremendous potential in disease diagnosis and prediction, providing a promising direction for clinical applications. Shan et al.[37] applied radiomics to the clinical prognosis assessment of subarachnoid hemorrhage, selecting 13 different features from 1316 radiomic features, thus constructing 7 machine learning models. The results show that the accuracy of prognosis assessment reached 0.88, proving that radiomic models have the potential to guide the prognosis prediction and treatment of subarachnoid hemorrhage. Xiang et al.[38] extracted and screened radiomic features from preoperative contrast-enhanced CT images of each patient, and the features after dimensionality reduction showed good performance in predicting the risk of gallbladder cancer prognosis at 1 year, 3 years, and 5 years. Li et al.[39] used a radiomic feature extraction method based on three selection factors, conducted experiments in 7 datasets containing 13 brain tumor classification tasks, and evaluated the overall performance using 5 metrics. The results show that radiomics has good classification performance, adaptability, and stability in brain tumor classification. Kumar et al.[40] extracted 42 radiomic features, including first-order and shape features, from a single cross-sectional image of T2-weighted imaging (T2WI), and used these features to build a robust machine learning model, achieving accurate grading of low-grade gliomas and high-grade gliomas. According to these studies, radiomics features can obtain more precise quantitative features compared to traditional radiological features, and can be widely used in disease identification diagnosis[41], grading and typing[42][43][44][45], and prognosis prediction[46][47][48], etc.

Previous studies have shown that radiomics methods can be effectively applied to the grading tasks of meningiomas. In 2019, Laukamp et al.[49] generated 990 radiomic features of shape and texture from MRI data of 46 grade I and 25 grade II untreated meningiomas, then inputted them into a multivariate logistic regression model after stepwise dimensionality reduction. The AUC for grading grade I and II meningiomas was 0.91, proving the feasibility of applying radiomic feature analysis to conventional MRI meningioma grading. Chen et al.[50] and Chu et al.[51] extracted several texture parameters from T1 CE images of meningioma patients (150 and 98 cases, respectively) in 2019 and 2020, applied these features to machine learning classifiers after feature selection to achieve accurate grading of meningiomas. These two studies proved that MRI radiomics methods based on T1 CE images have good predictive effects on meningioma grading, providing a basis for clinical treatment plan formulation. Additionally, in 2020, Han et al.[52] built 24 training models using 6 classifiers, thereby increasing the AUC to 0.956 for 27 test samples. In 2022, Guo et al.[53] focused on the edematous region, extracted a total of 851 radiomic features from tumors and edematous areas, and constructed models combining clinical information. The results show that the model combining edema features can achieve an AUC of 0.88 for meningioma grading, proving that radiological features of the edematous area may help in meningioma grading. Duan et al.[54] collected T1 CE images from 188 meningioma patients and built models using different machine learning methods. The results show that compared to other machine learning models, SVM and RF performed better, with relatively higher accuracy (0.79 and 0.77, respectively). In the same year, Duan et al.[55] developed a radiomics nomogram, increasing the accuracy to 0.86, further improving the feasibility of radiomics in clinical decision-making for meningiomas.

The effectiveness of radiomics in medical imaging classification tasks has been confirmed. However, it still requires manual intervention or additional feature engineering in the feature extraction process. In contrast, deep learning models automatically learn abstract feature representations, achieving automated feature learning and classification decisions through stacked neural networks. AlexNet[56], VGG[57], GoogLeNet[58] introduced deeper CNN structures and innovative feature extraction methods, significantly enhancing the model's expression and learning capabilities, marking milestones in the development of deep learning. ResNet[59] introduced residual connections to solve the gradient vanishing problem in deep network training, greatly improving training effects and performance. In recent years, high-performance models and their variants like ViT[60], Swin Transformer[61], and ConvNeXt[62] have made important breakthroughs in the field of image processing, advancing medical imaging classification. Lu et al.[63] proposed a ResNet based on pyramid dilated convolution for glioma classification. The results show that this method can effectively increase the receptive field of the original network, improving classification accuracy. Chen et al.[64] applied the self-attention mechanism in the Inception-Resnet structure, identifying CT diseases through classifiers, and assisted in the diagnostic process of novel coronavirus pneumonia (COVID-19), thereby further enhancing the classification performance of convolutional neural networks. Abdar[65] proposed a simple and novel hierarchical multi-level feature fusion model, containing an uncertainty-aware module, efficiently integrating original features with attention-based features. The accuracies in retinal OCT, lung CT, and chest X-ray medical image classification tasks reached 94.21%, 99.59%, and 96.50%, respectively, surpassing other state-of-the-art medical image classification methods. Zhou et al.[66] explored the impact of background color selection on the performance of deep models in skin disease classification by combining data preprocessing, data augmentation, and residual connections. The experimental results not only proved that the background information of color significantly affects the classification of skin diseases, but the classifiers trained on specific subsets also achieved state-of-the-art performance in recognizing black and red skin lesions. The studies indicate that deep learning-based classification models are another promising evaluation method, helping medical professionals more accurately analyze and interpret medical

images[67][68][69][70].

These research results prove that deep learning methods are an effective solution for medical image classification problems, and studies on meningioma grading based on deep learning technology have also rapidly emerged. Yang et al.[71] conducted a retrospective analysis in 2022, including 132 pathologically confirmed meningioma patients. They selected the largest slice of tumor lesions from the axial and sagittal directions of T1 WI and extracted a total of 15 radiomic and deep learning features, based on which they built a deep learning-radiomics model. On the test set, the model's AUC reached 0.935, proving that deep learning features can improve the performance of meningioma grading models. Vassantachart et al.[72] proposed a dual-input 3D CNN structure based on T1 CE and T2 Flair. The results show that the proposed model achieved a grading accuracy of 0.9 and an AUC of 0.91 in 96 meningioma samples. Compared to single modality, the multimodal fusion CNN structure significantly improved grading accuracy. In 2023, Liu et al.[73] combined high-dimensional 3D MRI imaging information and low-dimensional clinical data from 800 meningioma patients, proposing a multimodal deep fusion network. Specifically, the model used two specific branches to extract image and clinical features and utilized an image-clinical integration module to fuse these features. The experimental results show that this method achieved an AUC of 0.958 in meningioma grading, further proving the effectiveness of deep learning methods in meningioma grading.

III. Methodology

In this section, we introduce a novel network named 3D-MGNet, designed for the precise preoperative meningioma grading. This network incorporates dual modalities of MRI data: T1 CE and T2 Flair, enhancing the ability to extract the multimodal imaging data characteristic within meningiomas, enabling accurate grading. The 3D-MGNet consists of a Dual Multimodal Meningioma Feature Extractor (DME), followed by deep-radiomecs features integration discriminator for robust meningiomas grading. Within DME, a novel 3D-LKA mechanism is also incorporated, aiming at enhancing the precision of meningiomas grading. As validated across significant experiments, the proposed methodology exhibits notable improvements over previous approaches.

A. Overview of 3D-MGNet Architecture

The architecture of 3D-MGNet is designed to enhance meningioma grading accuracy through the DME. As shown in Fig. 1. This module operates on a dual-branch input system, processing T1 CE and T2 Flair modalities, denoted as $F_{\text{T1 CE}}$ and $F_{\text{T2 Flair}}$ respectively. By exploiting the distinct characteristics captured by each modality, the network significantly improves the accuracy of grading. More specifically, Res-LKA Blocks are Central to the feature extraction process, denoted as Res-LKA(F). This module is utilized across four downsampling layers within the DME. Each layer contains two Res-LKA blocks, working sequentially to refine and enhance the extracted features F through LKA attention mechanism. This mechanism is designed to capture the long-range dependencies of MRI images efficiently, enabling the network to focus on the most salient features relevant to meningioma grading. Following the feature extraction phase, the architecture incorporates a deep-radiomecs features integration discriminator. This component confuses the Radiomics information into deep feature, ensuring robust classification outcomes.

B. 3D-LKA

The 3D-LKA mechanism is an innovative component of the 3D-MGNet architecture designed to enhance attention to salient features in 3D meningioma imaging. The structure of 3D-LKA is shown in Fig. 2. It integrates spatial local and long-distance convolution operations to efficiently process 3D data, capturing both local details and global context. The mechanism comprises three key elements: spatial local convolution operations for detailed feature extraction, spatial long-distance convolution operations to capture extended spatial relationships, and channel convolution operations to integrate information across different feature channels. This structure allows the 3D-LKA to adaptively adjust its output based on input features, focusing on important areas without the need for traditional normalization methods like Sigmoid or Softmax, thus offering a balanced approach to both local and global attention within 3D medical images.

The attention mechanism within the Res-LKA Block is formalized as follows:

$$\text{Attention} = \text{Conv}_{1\times1}(\text{DW-D-Conv}(\text{DW-Conv}(F))) \quad (1)$$

where $F \in \mathbb{R}^{C\times H\times W}$ represents the input features, DW-Conv denotes depthwise convolution, DW-D-Conv is the depthwise dilated convolution for capturing long-distance spatial relationships, and $\text{Conv}_{1\times1}$ is used to integrate channel-wise information. The output can be formulated as Attention $\in \mathbb{R}^{C\times H\times W}$, which is the attention feature map highlighting the importance of each feature.

The feature integration within the block is described by:

$$\text{Out} = \text{Attention} \odot F \quad (2)$$

where $\odot$ denotes element-wise multiplication, facilitating the modulation of input features F by the attention map to emphasize salient features.

C. 3D-Res-LAK Block

The 3D-Res-LKA Block (as shown in Fig. 3.) is designed to enhance feature extraction capabilities for 3D medical feature, capturing both local and global contextual information efficiently. Moreover, this block combines the strengths of residual learning with the 3D-LKA mechanism to process volumetric data effectively. The specific block operations can be summarized as follows:

$$F' = \text{LKAB}(\text{BN}(\text{Conv}_{3\times3\times3}(F_{\text{in}}))) \quad (3)$$

$$F'' = \text{BN}(\text{Conv}_{3\times3\times3}(\text{ReLU}(F'))) \quad (4)$$

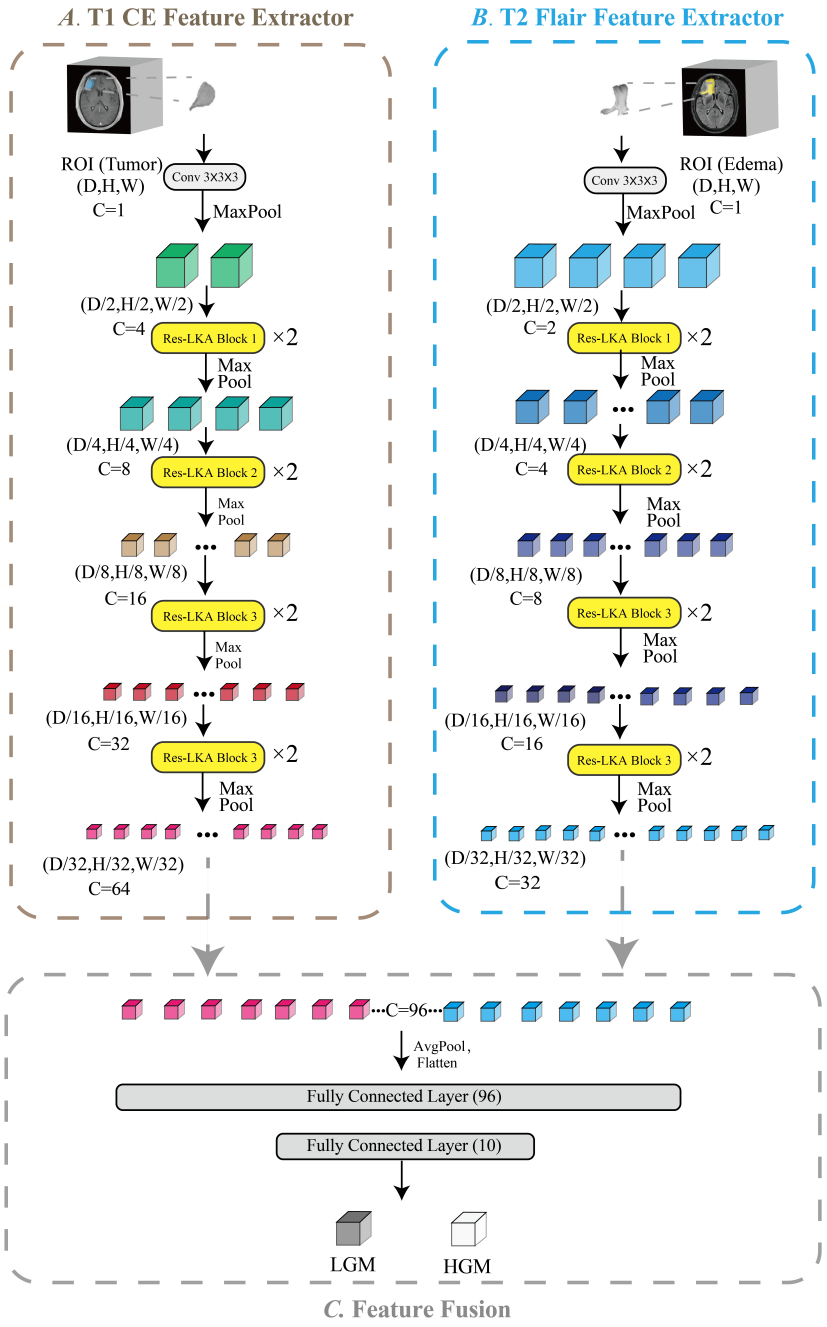

Fig. 1: Schematic diagram of 3D MGNet.

$$F_{\text{out}} = \text{ReLU}(F'') + F_{\text{in}} \tag{5}$$

Here, F_{in} and F_{out} are the input and output features of the block, respectively, LKAB represents the operations within the 3D-LKA block, BN is batch normalization, and ReLU is the activation function.

Moreover, the 3D-LKA block within the Res-LKA module is designed to refine feature maps while preserving spatial resolution and channel dimensions. The input feature map, X_{in}, first passes through a 1×1 convolution, enhancing channel-wise features while maintaining spatial dimensions. This is followed by the application of a GELU nonlinearity to introduce complex, non-linear transformations conducive to deep learning tasks:

$$X_1 = GELU(Conv_{1\times1}(X_{in})) \tag{6}$$

Subsequently, X_1 is processed by the LKA mechanism, which enriches the feature map by capturing both local and long-

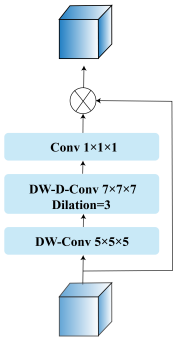

Fig. 2: Schematic diagram of 3D-LKA.

distance spatial relationships:

$$X_{LKA} = LKA(X_1) \tag{7}$$

Finally, the output X_{out} is computed by performing another 1×1 convolution on X_{LKA} and adding the result to the original input X_{in}, employing a residual connection that aids in preserving important features and combating the vanishing gradient problem:

$$X_{out} = Conv_{1\times1}(X_{LKA}) + X_{in} \tag{8}$$

In conclusion, the 3D Res-LKA Block is a novel contribution to the field of deep learning for medical imaging, particularly for the grading of meningiomas. Its design emphasizes the importance of attention mechanisms in capturing complex spatial relationships within volumetric data, offering a significant improvement over traditional models. By integrating both local and global contextual information through a mathematically rigorous framework, the Res-LKA Block enhances the model's ability to discern subtle differences in tumor characteristics, potentially leading to more accurate and reliable grading outcomes.

D. Dual Multimodal Meningioma Feature Extractor

The Dual Multimodal Meningioma Feature Extractor within the 3D MGNet utilizes a dual-branch strategy to process MRI data from T1 CE and T2 Flair modalities. The architecture employs a series of 3×3×3 convolutional layers to reduce the input image dimension $D \times H \times W$ by half across each dimension, resulting in a feature size of $\frac{D}{2} \times \frac{H}{2} \times \frac{W}{2}$, where D, H, and W represent depth, height, and width, respectively. This is followed by four downsampling layers, each comprising two Res-LKA Blocks for deep feature extraction. The convolutional complexity and expressiveness for each MRI sequence branch are tailored by varying the number of convolutional kernels, with max pooling applied for feature map resolution reduction. The network's asymmetric CNN structure gives a higher weight ratio to T1 CE (2:1) compared to T2 Flair, with channel outputs after each layer of Res-LKA Blocks as (T1 CE: 4, 8, 16, 32; T2 Flair: 8, 16, 32, 64). This configuration enables the network to extract rich information from the T1 CE sequences while integrating features from T2 Flair. A Softmax function is applied to the features obtained from average pooling and flattening operations to map them to binary classifications, optimizing the network for precise meningioma grading. This Multimodel approach with novel attention mechanisms significantly enhances the accuracy of meningioma grading, providing a robust tool for assisting the grading of meningioma.

E. Radiomics-deep features integration discriminator

A significant challenge in machine learning the propensity to overfit, which limits the ability of model to effectively identify salient features under unfamiliar conditions. To mitigate this issue, we propose a radiomic feature extraction framework (RFEF) that consists of traditional feature extraction techniques to provide supplementary characteristics for the discriminator. This approach enhances the stability and robustness of the model, effectively extracting relevant features crucial for accurate tumor grading even in new or varying data conditions.

Specifically, radiomic features are initially extracted from segmented regions of interest (ROIs) within T1 CE and T2 FLAIR MRI images using software 3D Slicer. These features encompass shape, first-order statistics, textures, and wavelet-transformed attributes. To ensure the reliability and stability the extracted features, an Intraclass Correlation Coefficient (ICC) pre-selection is applied, where features with ICC values below a certain threshold are discarded. Subsequently, the remaining features undergo dimensionality reduction through Principal Component Analysis (PCA). This process transforms the high-dimensional feature set into a lower-dimensional space, preserving the significant variance in the feature.

Mathmatically, given a feature matrix $X \in \mathbb{R}^{m\times n}$, where m is the number of features and n is the number of samples, PCA seeks to find a matrix $W \in \mathbb{R}^{m\times k}$ that maps X to a new feature space $Y \in \mathbb{R}^{k\times n}$:

$$Y = W^T X \tag{9}$$

The columns of W are the eigenvectors of the covariance matrix $X^T X$ associated with the largest eigenvalues.

The radiomic features selected by PCA are then integrated with deep features from the neural network. Let F_{deep} denotes the deep feature vector extracted from the neural network, and F_{rad} denote the radiomic feature vector after dimensionality reduction. The integrated feature vector F_{int} can be represented as:

$$F_{\text{int}} = F_{\text{deep}} + F_{\text{rad}} \tag{10}$$

The integrated feature vector F_{int} is then fed into a discriminator function D, which consists of a series of fully connected layers as depicted in the neural network architecture. Initially, F_{int} passes through a fully connected layer with 96 neurons, designed to further synthesize and compact the information. The process continues with the feature vector then being relayed to a subsequent fully connected layer

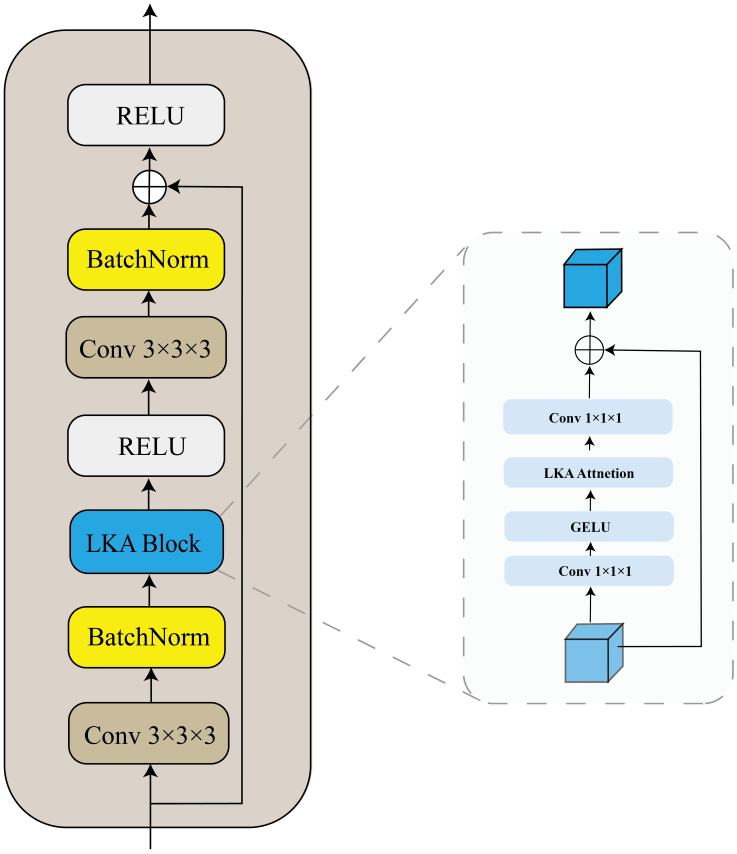

Fig. 3: Schematic diagram of 3D-Res-LAK Block.

consisting of 10 neurons. This layer acts as the penultimate stage in the decision-making process, preparing the data for final classification. Ultimately, the outcome of the last fully connected layer undergoes a softmax activation that assigns probabilities to each category of meningioma grades, effectively distinguishing between low-grade meningiomas (LGM) and high-grade meningiomas (HGM). The final prediction is made based on the highest probability, thereby classifying the meningioma grade with enhanced precision through the discriminative capabilities of the neural network.

IV. Experiment

A. Preprocessing

The dataset utilized in this experiment comprises ROI-segmented 3D images from T1 CE and T2 FLAIR sequences. Compared to traditional 2D slices, 3D images provide richer spatial information, effectively capturing the morphology, size, and position of meningiomas. However, due to variations in scanning equipment and parameters, the raw 3D images have different voxel sizes, which could negatively affect network training and performance. Consequently, we resampled the meningioma 3D images in this proposal. Specifically, we adjusted the slice thickness in the z-direction and the inter-slice spacing in the x and y directions to ensure uniform voxel dimensions across all samples. This spatial standardization minimizes information loss due to resolution differences, enhancing network performance and robustness. Furthermore, to reduce computational and storage costs, the dimensions of meningioma images are resized to $128\times128\times128$. To mitigate brightness and contrast differences caused by varying scanning equipment and parameters, which helps the network more easily learn useful features, image normalization is performed to reduce the impact of noise and outliers in the dataset for network training.

B. Experiment setting

The experiments are conducted on a system running Windows 10, utilizing Pytorch 1.7.0 and CUDA 10.1. During the training process, all algorithms are optimized using the Adam optimizer to ensure convergence, with the learning rate set at 0.001 and the minimum batch size configured to 2. The models are trained over 100 epochs on an NVIDIA Tesla V100 GPU, employing CrossEntropy Loss as the objective function for learning.

C. Comparative Experiment

Given the constraints of computational performance and the limited number of deep learning models for 3D image

classification currently available, this study exhibits the comparative analysis to the 3D versions of VGG (VGG16 and VGG19) and ResNet (ResNet18 and ResNet50), validating both single-branch (Single) and dual-branch (Dual) grading results. The Single setup included four models—VGG16, VGG19, ResNet18, and ResNet50—each running eight separate comparative experiments using T1 CE and T2 Flair modalities. In the Dual setup, both T1 CE and T2 Flair branches utilize the same backbone network, specifically configured as Dual-VGG16, Dual-VGG19, Dual-ResNet18, and Dual-ResNet50. As shown in Table I, single-branch networks significantly underperformed in comparison to dual-branch networks, especially in the recognition of HGM. The ACC for Single-VGG16 and Single-ResNet18 is 0.457 and 0.400 respectively, indicating that a single modality is insufficient for extracting meningioma grading features adequately. In contrast, dual-branch models exhibit substantial improvements, with AUCs of 0.768 and 0.728 for Dual-VGG16 and Dual-ResNet18 respectively. Nevertheless, Dual-VGG19 and Dual-ResNet50 with deeper network structures and more convolutional kernels fail to outperform their less streamlined version, indicating that more complex networks disadvantage classifying small-sample medical images. The proposed 3D MGNet outperformed these models across all metrics for both LGM and HGM categories. In the absence of radiomic feature integration, the baseline performed with precision (PRE) rates of 0.870 and 0.750, sensitivity (SEN) rates of 0.870 and 0.750, specificity (SPE) rates of 0.750 and 0.870, and an AUC reaching 0.886, validating the effectiveness of the proposed approach.

D. Ablation Study

The ablation studies are exhibited to investigate the impact of the dual-branch ratio configuration on the meningiomas grading performance. Performance metrics obtained from four experimental setups are showcased in Table II. The results revealed that using only branch 1 (i.e., the T1 CE branch), the F1 scores for LGM and HGM are 0.714 and 0.571, respectively. These scores reflect a decline of 0.156 and 0.179 compared to the asymmetric dual-branch structure (Ours), which scored an F1 of 0.870 for LGM and 0.750 for HGM. Furthermore, the AUC achieved by branch 1 was 0.716, which is a reduction of 0.17 from the proposed structure's AUC of 0.886. In cases where only branch 2 (i.e., the T2 Flair branch) was used, the F1 scores were even lower, with LGM at 0.619 and HGM at 0.429, indicating significant decreases of 0.251 and 0.321 from the dual-branch structure's performance. This demonstrates that branch 1 contains richer feature information within the tumor region than branch 2. To validate the efficacy of the asymmetrical ratio, we compared it with a symmetrical dual-input structure, averaging the channel numbers of downsampled layers in 3D MGNet (6, 12, 24, 48 respectively). The symmetrical structure achieved an ACC of 0.743 and an AUC of 0.748, marking improvements over the individual branches. Specifically, this represents increases of 0.086 and 0.032 over branch 1, and 0.2 and 0.07 over branch 2, substantiating the benefits of multimodal and multi-information fusion. However, the 3D MGNet demonstrated enhancements across all assessment metrics compared to the symmetrical structure, substantiating that an asymmetrical structure with a higher tumor weighting can synthesize a richer set of features, thus improving the accuracy of meningioma grading.

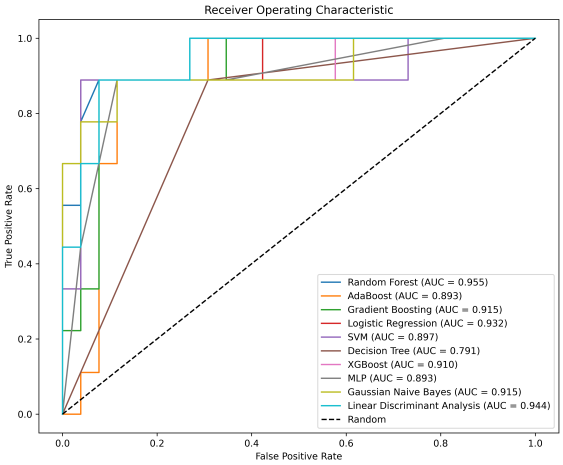

Fig. 4: ROC curves of the fused depth features and radiomics feature.

E. Integration of Deep Learning and Radiomics Features

To enhance the performance of the meningioma grading model, this study extracts quantitative deep features from the second layer of the fully connected layers (as shown in Fig. 1 , Fully Connected Layer (10)). These outputs serve as a higher-level representation of the input data, endowed with richer semantic information.

Due to the second layer's output nodes being set to 10, the number of features included is relatively small; therefore, no feature selection process is conducted. After standardizing the deep features and performing other preprocessing procedures, these features are then fused with the radiomics features. Finally, a machine learning classifier is utilized to predict the meningioma grade based on the integrated features. This fusion of deep learning and radiomics leads to a more robust and accurate grading of meningiomas, tapping into the comprehensive capabilities of both deep feature representations and the detailed characteristics captured by radiomics.

Fig. 4 demonstrate the ROC curves of the fused depth features and radiomics features, and the results show that the grading performance of all models is significantly improved. There is no significant data difference in AUC between the models, which are 0.955 (Random Forest), 0.893 (AdaBoost), 0.915 (Gradient Boosting), 0.932 (Logistic Regression), and 0.897 (SVM). This shows the effectiveness of feature fusion.

Table IV shows the quantitative grading results of fusing deep learning features and radiomics features. The evaluation results of all the models are excellent, with an accuracy (ACC) of 0.943 (Random Forest), 0.857 (AdaBoost), 0.914 (Gradient Boosting), 0.914 (Logistic Regression), and 0.886 (SVM),

TABLE I: Comparative experiments with other 3D classification models

Model	Modality	Category	PRE	SEN	SPE	F1	ACC	AUC
Single-VGG16	T1-CE	LGM	0.625	0.435	0.500	0.513	0.457	0.531
		HGM	0.316	0.435	0.500	0.367		
	T2-Flair	LGM	0.625	0.435	0.500	0.513	0.457	0.531
		HGM	0.316	0.435	0.500	0.367		
Single-VGG19	T1-CE	LGM	0.722	0.565	0.583	0.634	0.571	0.678
		HGM	0.412	0.583	0.565	0.483		
	T2-Flair	LGM	0.720	0.783	0.417	0.750	0.657	0.698
		HGM	0.500	0.417	0.783	0.455		
Single-ResNet18	T1-CE	LGM	0.563	0.391	0.417	0.462	0.400	0.586
		HGM	0.263	0.417	0.391	0.323		
	T2-Flair	LGM	0.750	0.522	0.667	0.615	0.571	0.659
		HGM	0.421	0.667	0.522	0.516		
Single-ResNet50	T1-CE	LGM	0.667	0.870	0.167	0.755	0.629	0.503
		HGM	0.400	0.167	0.870	0.235		
	T2-Flair	LGM	0.786	0.478	0.750	0.595	0.571	0.598
		HGM	0.429	0.750	0.478	0.545		
Dual-VGG16	multimodal information	LGM	0.850	0.739	0.750	0.791	0.743	0.768
		HGM	0.600	0.750	0.739	0.667		
Dual-VGG19	multimodal information	LGM	0.762	0.696	0.583	0.727	0.657	0.719
		HGM	0.500	0.583	0.696	0.538		
Dual-ResNet18	multimodal information	LGM	0.783	0.783	0.583	0.783	0.714	0.728
		HGM	0.583	0.583	0.783	0.583		
Dual-ResNet50	multimodal information	LGM	0.765	0.565	0.667	0.650	0.600	0.703
		HGM	0.444	0.667	0.565	0.533		
3D MGNet	multimodal information	LGM	0.870	0.870	0.750	0.870	0.829	0.886
		HGM	0.750	0.750	0.870	0.750		

TABLE II: Experimental ablation of model branches

Model Structure	Modality	Category	PRE	SEN	SPE	F1	ACC	AUC
Branch T1-CE	multimodal information	LGM	0.789	0.652	0.667	0.714	0.657	0.716
		HGM	0.500	0.667	0.652	0.571		
Branch T2-Flair	multimodal information	LGM	0.684	0.565	0.500	0.619	0.543	0.678
		HGM	0.375	0.500	0.565	0.429		
Symmetry	multimodal information	LGM	0.818	0.783	0.667	0.800	0.743	0.748
		HGM	0.615	0.667	0.783	0.640		
3D MGNet	multimodal information	LGM	0.870	0.870	0.750	0.870	0.829	0.886
		HGM	0.750	0.750	0.870	0.750		

TABLE III: Ablation experiments on the LKA module.

Model Structure	Modality	Category	PRE	SEN	SPE	F1	ACC	AUC
No LKA module	multimodal information	LGM	0.864	0.826	0.750	0.844	0.800	0.867
		HGM	0.692	0.750	0.826	0.720		
Have LKA module	multimodal information	LGM	0.870	0.870	0.750	0.870	0.829	0.886
		HGM	0.750	0.750	0.870	0.750		

respectively. In addition, the machine learning model that combines deep learning and radiomics features has improved the recognition accuracy of HGM. This result demonstrates that deep radiomics features can effectively mitigate the performance imbalance problem due to sample imbalance.

V. Conclusion

This work introduces a multimodal medical network named 3D-MGNet that significantly improves the accuracy of preoperative meningioma grading. Through the integration of radiomics and deep learning techniques, the robustness and precision of the prediction results have been effectively ensured. Furthermore, the LKA attention mechanism within the network ensures efficiency in tumor grading while capturing long-frequency contexture, making it more effectively applicable to preoperative diagnosis.

References

[1] Y. W. Park, J. Oh, S. C. You, K. Han, S. S. Ahn, Y. S. Choi, J. H. Chang, S. H. Kim, and S.-K. Lee, "Radiomics and machine learning may accurately predict the grade and histological subtype in meningiomas using conventional and diffusion tensor imaging," *European radiology*, vol. 29, pp. 4068–4076, 2019.

[2] D. N. Louis, A. Perry, G. Reifenberger, A. Von Deimling, D. Figarella-Branger, W. K. Cavenee, H. Ohgaki, O. D. Wiestler, P. Kleihues, and D. W. Ellison, "The 2016 world health organization classification of tumors of the central nervous system: a summary," *Acta neuropathologica*, vol. 131, pp. 803–820, 2016.

[3] J. Rees, J. Smirniotopoulos, and R. Jones, "World health organization classification of central nervous system tumors," in

TABLE IV: Experimental ablation of model branches

Model Structure	Feature	Category	PRE	SEN	SPE	F1	ACC	AUC	95% CI
Random Forest	Radiomic	LGM	0.909	0.870	0.833	0.889	0.857	0.846	(0.697, 0.992)
		HGM	0.769	0.883	0.870	0.800			
	Deep learning fused radiomics	LGM	0.957	0.957	0.917	0.957	0.943	0.955	(0.892, 1.000)
		HGM	0.917	0.917	0.957	0.917			
AdaBoost	Radiomic	LGM	0.905	0.826	0.833	0.864	0.829	0.902	(0.701, 1.000)
		HGM	0.500	0.667	0.652	0.571			
	Deep learning fused radiomics	LGM	0.909	0.870	0.833	0.889	0.857	0.893	(0.762, 1.000)
		HGM	0.714	0.833	0.826	0.769			
Gradient Boosting	Radiomic	LGM	0.913	0.913	0.833	0.913	0.886	0.917	(0.808, 1.000)
		HGM	0.833	0.833	0.913	0.833			
	Deep learning fused radiomics	LGM	0.955	0.913	0.917	0.933	0.914	0.915	(0.833, 1.000)
		HGM	0.846	0.917	0.913	0.880			
Logistic Regression	Radiomic	LGM	0.783	0.783	0.583	0.783	0.714	0.822	(0.674, 0.956)
		HGM	0.583	0.583	0.783	0.583			
	Deep learning fused radiomics	LGM	0.917	0.957	0.833	0.936	0.914	0.932	(0.852, 1.000)
		HGM	0.909	0.833	0.957	0.870			
SVM	Radiomic	LGM	0.808	0.913	0.583	0.857	0.800	0.862	(0.723, 1.000)
		HGM	0.778	0.583	0.913	0.667			
	Deep learning fused radiomics	LGM	0.880	0.957	0.750	0.917	0.886	0.897	(0.756, 1.000)
		HGM	0.900	0.750	0.957	0.818			

RADIOLOGY, vol. 201. RADIOLOGICAL SOC NORTH AMER 20TH AND NORTHAMPTON STS, EASTON, PA 18042, 1996, pp. 77–77.

[4] L. Rogers, I. Barani, M. Chamberlain, T. J. Kaley, M. McDermott, J. Raizer, D. Schiff, D. C. Weber, P. Y. Wen, and M. A. Vogelbaum, "Meningiomas: knowledge base, treatment outcomes, and uncertainties. a rano review," *Journal of neurosurgery*, vol. 122, no. 1, pp. 4–23, 2015.

[5] R. Goldbrunner, G. Minniti, M. Preusser, M. D. Jenkinson, K. Sallabanda, E. Houdart, A. von Deimling, P. Stavrinou, F. Lefranc, M. Lund-Johansen *et al.*, "Eano guidelines for the diagnosis and treatment of meningiomas," *The Lancet Oncology*, vol. 17, no. 9, pp. e383–e391, 2016.

[6] I. R. Whittle, C. Smith, P. Navoo, and D. Collie, "Meningiomas," *The Lancet*, vol. 363, no. 9420, pp. 1535–1543, 2004.

[7] L. Bertero, G. Dalla Dea, S. Osella-Abate, C. Botta, I. Castellano, I. Morra, B. Pollo, C. Calatozzolo, S. Patriarca, C. Mantovani *et al.*, "Prognostic characterization of higher-grade meningiomas: a histopathological score to predict progression and outcome," *Journal of Neuropathology & Experimental Neurology*, vol. 78, no. 3, pp. 248–256, 2019.

[8] M. J. Riemenschneider, A. Perry, and G. Reifenberger, "Histological classification and molecular genetics of meningiomas," *The Lancet Neurology*, vol. 5, no. 12, pp. 1045–1054, 2006.

[9] S. Schob, C. Frydrychowicz, M. Gawlitza, L. Bure, M. Preuß, K.-T. Hoffmann, and A. Surov, "Signal intensities in preoperative mri do not reflect proliferative activity in meningioma," *Translational oncology*, vol. 9, no. 4, pp. 274–279, 2016.

[10] M. Nowosielski, N. Galldiks, S. Iglseder, P. Kickingereder, A. Von Deimling, M. Bendszus, W. Wick, and F. Sahm, "Diagnostic challenges in meningioma," *Neuro-oncology*, vol. 19, no. 12, pp. 1588–1598, 2017.

[11] S. Saraf, B. J. McCarthy, and J. L. Villano, "Update on meningiomas," *The oncologist*, vol. 16, no. 11, pp. 1604–1613, 2011.

[12] J. Halliday, S. A. Rutherford, M. G. McCabe, and D. G. Evans, "An update on the diagnosis and treatment of vestibular schwannoma," *Expert review of neurotherapeutics*, vol. 18, no. 1, pp. 29–39, 2018.

[13] T. Hashiba, N. Hashimoto, M. Maruno, S. Izumoto, T. Suzuki, N. Kagawa, and T. Yoshimine, "Scoring radiologic characteristics to predict proliferative potential in meningiomas," *Brain tumor pathology*, vol. 23, pp. 49–54, 2006.

[14] Y. Kawahara, M. Nakada, Y. Hayashi, Y. Kai, Y. Hayashi, N. Uchiyama, H. Nakamura, J.-i. Kuratsu, and J.-i. Hamada, "Prediction of high-grade meningioma by preoperative mri assessment," *Journal of neuro-oncology*, vol. 108, pp. 147–152, 2012.

[15] B.-J. Lin, K.-N. Chou, H.-W. Kao, C. Lin, W.-C. Tsai, S.-W. Feng, M.-S. Lee, and D.-Y. Hueng, "Correlation between magnetic resonance imaging grading and pathological grading in meningioma," *Journal of neurosurgery*, vol. 121, no. 5, pp. 1201–1208, 2014.

[16] A. T. Hale, L. Wang, M. K. Strother, and L. B. Chambless, "Differentiating meningioma grade by imaging features on magnetic resonance imaging," *Journal of Clinical Neuroscience*, vol. 48, pp. 71–75, 2018.

[17] R. Y. Huang, W. L. Bi, B. Griffith, T. J. Kaufmann, C. la Fougère, N. O. Schmidt, J. C. Tonn, M. A. Vogelbaum, P. Y. Wen, K. Aldape *et al.*, "Imaging and diagnostic advances for intracranial meningiomas," *Neuro-oncology*, vol. 21, no. Supplement_1, pp. i44–i61, 2019.

[18] D. C. Spille, P. B. Sporns, K. Hess, W. Stummer, and B. Brokinkel, "Prediction of high-grade histology and recurrence in meningiomas using routine preoperative magnetic resonance imaging: a systematic review," *World neurosurgery*, vol. 128, pp. 174–181, 2019.

[19] C. Ke, H. Chen, X. Lv, H. Li, Y. Zhang, M. Chen, D. Hu, G. Ruan, Y. Zhang, Y. Zhang *et al.*, "Differentiation between benign and nonbenign meningiomas by using texture analysis from multiparametric mri," *Journal of Magnetic Resonance Imaging*, vol. 51, no. 6, pp. 1810–1820, 2020.

[20] R. M. Judd, "Machine learning in medical imaging: all journeys begin with a single step," pp. 696–698, 2020.

[21] M. L. Giger, "Machine learning in medical imaging," *Journal of the American College of Radiology*, vol. 15, no. 3, pp. 512–520, 2018.

[22] P. Lambin, R. T. Leijenaar, T. M. Deist, J. Peerlings, E. E. De Jong, J. Van Timmeren, S. Sanduleanu, R. T. Larue, A. J. Even, A. Jochems *et al.*, "Radiomics: the bridge between medical imaging and personalized medicine," *Nature reviews Clinical oncology*, vol. 14, no. 12, pp. 749–762, 2017.

[23] P. Lambin, E. Rios-Velazquez, R. Leijenaar, S. Carvalho, R. G. Van Stiphout, P. Granton, C. M. Zegers, R. Gillies, R. Boellard, A. Dekker *et al.*, "Radiomics: extracting more information from medical images using advanced feature analysis," *European journal of cancer*, vol. 48, no. 4, pp. 441–446, 2012.

[24] Y. Lu, L. Liu, S. Luan, J. Xiong, D. Geng, and B. Yin, "The

diagnostic value of texture analysis in predicting who grades of meningiomas based on adc maps: an attempt using decision tree and decision forest," *European radiology*, vol. 29, pp. 1318–1328, 2019.

[25] P.-F. Yan, L. Yan, T.-T. Hu, D.-D. Xiao, Z. Zhang, H.-Y. Zhao, and J. Feng, "The potential value of preoperative mri texture and shape analysis in grading meningiomas: a preliminary investigation," *Translational oncology*, vol. 10, no. 4, pp. 570–577, 2017.

[26] X. Li, Y. Miao, L. Han, J. Dong, Y. Guo, Y. Shang, L. Xie, Q. Song, and A. Liu, "Meningioma grading using conventional mri histogram analysis based on 3d tumor measurement," *European Journal of Radiology*, vol. 110, pp. 45–53, 2019.

[27] M.-H. Guo, C.-Z. Lu, Z.-N. Liu, M.-M. Cheng, and S.-M. Hu, "Visual attention network," *Computational Visual Media*, vol. 9, no. 4, pp. 733–752, 2023.

[28] M. E. Mayerhoefer, A. Materka, G. Langs, I. Häggström, P. Szczypiński, P. Gibbs, and G. Cook, "Introduction to radiomics," *Journal of Nuclear Medicine*, vol. 61, no. 4, pp. 488–495, 2020.

[29] A. A. Ardakani, N. J. Bureau, E. J. Ciaccio, and U. R. Acharya, "Interpretation of radiomics features–a pictorial review," *Computer methods and programs in biomedicine*, vol. 215, p. 106609, 2022.

[30] R. M. Judd, "Machine learning in medical imaging: all journeys begin with a single step," pp. 696–698, 2020.

[31] M. L. Giger, "Machine learning in medical imaging," *Journal of the American College of Radiology*, vol. 15, no. 3, pp. 512–520, 2018.

[32] T. M. Devi, G. Ramani, and S. X. Arockiaraj, "Mr brain tumor classification and segmentation via wavelets," in *2018 International Conference on Wireless Communications, Signal Processing and Networking (WiSPNET)*. IEEE, 2018, pp. 1–4.

[33] A. R. Mathew and P. B. Anto, "Tumor detection and classification of mri brain image using wavelet transform and svm," in *2017 International conference on signal processing and communication (ICSPC)*. IEEE, 2017, pp. 75–78.

[34] F. Polly, S. Shil, M. A. Hossain, A. Ayman, and Y. M. Jang, "Detection and classification of hgg and lgg brain tumor using machine learning," in *2018 International Conference on Information Networking (ICOIN)*. IEEE, 2018, pp. 813–817.

[35] A. Islam, M. F. Hossain, and C. Saha, "A new hybrid approach for brain tumor classification using bwt-ksvm," in *2017 4th International Conference on Advances in Electrical Engineering (ICAEE)*. IEEE, 2017, pp. 241–246.

[36] J. P. O'Connor, "Cancer heterogeneity and imaging," in *Seminars in cell & developmental biology*, vol. 64. Elsevier, 2017, pp. 48–57.

[37] D. Shan, J. Wang, P. Qi, J. Lu, and D. Wang, "Non-contrasted ct radiomics for sah prognosis prediction," *Bioengineering*, vol. 10, no. 8, p. 967, 2023.

[38] F. Xiang, X. Liang, L. Yang, X. Liu, and S. Yan, "Contrast-enhanced ct radiomics for prediction of recurrence-free survival in gallbladder carcinoma after surgical resection," *European Radiology*, vol. 32, no. 10, pp. 7087–7097, 2022.

[39] L. Li, M. Wang, X. Jiang, and Y. Lin, "Universal multi-factor feature selection method for radiomics-based brain tumor classification," *Computers in Biology and Medicine*, vol. 164, p. 107122, 2023.

[40] A. Kumar, A. K. Jha, J. P. Agarwal, M. Yadav, S. Badhe, A. Sahay, S. Epari, A. Sahu, K. Bhattacharya, A. Chatterjee *et al.*, "Machine-learning-based radiomics for classifying glioma grade from magnetic resonance images of the brain," *Journal of Personalized Medicine*, vol. 13, no. 6, p. 920, 2023.

[41] X. Zhang, C. Cui, S. Zhao, L. Xie, and Y. Tian, "Cardiac magnetic resonance radiomics for disease classification," *European Radiology*, vol. 33, no. 4, pp. 2312–2323, 2023.

[42] Y. Bian, H. Jiang, C. Ma, L. Wang, J. Zheng, G. Jin, and J. Lu, "Ct-based radiomics score for distinguishing between grade 1 and grade 2 nonfunctioning pancreatic neuroendocrine tumors," *American Journal of Roentgenology*, vol. 215, no. 4, pp. 852–863, 2020.

[43] Y. Zhang, Y. Zhu, X. Shi, J. Tao, J. Cui, Y. Dai, M. Zheng, and S. Wang, "Soft tissue sarcomas: preoperative predictive histopathological grading based on radiomics of mri," *Academic Radiology*, vol. 26, no. 9, pp. 1262–1268, 2019.

[44] W. You, Y. Mao, X. Jiao, D. Wang, J. Liu, P. Lei, and W. Liao, "The combination of radiomics features and vasari standard to predict glioma grade," *Frontiers in Oncology*, vol. 13, p. 1083216, 2023.

[45] Y. Yao, Y. Zhao, L. Lu, Y. Zhao, X. Lin, J. Xia, X. Zheng, Y. Shen, Z. Cai, Y. Li *et al.*, "Prediction of histopathologic grades of myxofibrosarcoma with radiomics based on magnetic resonance imaging," *Journal of Cancer Research and Clinical Oncology*, vol. 149, no. 12, pp. 10 169–10 179, 2023.

[46] F. Cousin, T. Louis, S. Dheur, F. Aboubakar, B. Ghaye, M. Occhipinti, W. Vos, F. Bottari, A. Paulus, A. Sibille *et al.*, "Radiomics and delta-radiomics signatures to predict response and survival in patients with non-small-cell lung cancer treated with immune checkpoint inhibitors," *Cancers*, vol. 15, no. 7, p. 1968, 2023.

[47] Y. Wang, W. Liu, Y. Yu, J.-j. Liu, H.-d. Xue, Y.-f. Qi, J. Lei, J.-c. Yu, and Z.-y. Jin, "Ct radiomics nomogram for the preoperative prediction of lymph node metastasis in gastric cancer," *European radiology*, vol. 30, pp. 976–986, 2020.

[48] J. Liu, J. Tang, B. Xia, Z. Gu, H. Yin, H. Zhang, H. Yang, and B. Song, "Novel radiomics-clinical model for the noninvasive prediction of new fractures after vertebral augmentation," *Academic Radiology*, vol. 30, no. 6, pp. 1092–1100, 2023.

[49] K. R. Laukamp, G. Shakirin, B. Baeßler, F. Thiele, D. Zopfs, N. G. Hokamp, M. Timmer, C. Kabbasch, M. Perkuhn, and J. Borggrefe, "Accuracy of radiomics-based feature analysis on multiparametric magnetic resonance images for noninvasive meningioma grading," *World Neurosurgery*, vol. 132, pp. e366–e390, 2019.

[50] C. Chen, X. Guo, J. Wang, W. Guo, X. Ma, and J. Xu, "The diagnostic value of radiomics-based machine learning in predicting the grade of meningiomas using conventional magnetic resonance imaging: a preliminary study," *Frontiers in oncology*, vol. 9, p. 1338, 2019.

[51] H. Chu, X. Lin, J. He, P. Pang, B. Fan, P. Lei, D. Guo, and C. Ye, "Value of mri radiomics based on enhanced t1wi images in prediction of meningiomas grade," *Academic radiology*, vol. 28, no. 5, pp. 687–693, 2021.

[52] Y. Han, T. Wang, P. Wu, H. Zhang, H. Chen, and C. Yang, "Meningiomas: Preoperative predictive histopathological grading based on radiomics of mri," *Magnetic Resonance Imaging*, vol. 77, pp. 36–43, 2021.

[53] Z. Guo, Z. Tian, F. Shi, P. Xu, J. Zhang, C. Ling, and Q. Zeng, "Radiomic features of the edema region may contribute to grading meningiomas with peritumoral edema," *Journal of Magnetic Resonance Imaging*, vol. 58, no. 1, pp. 301–310, 2023.

[54] C. Duan, N. Li, Y. Li, F. Liu, J. Wang, X. Liu, and W. Xu, "Comparison of different radiomic models based on enhanced t1-weighted images to predict the meningioma grade," *Clinical Radiology*, vol. 77, no. 4, pp. e302–e307, 2022.

[55] C. Duan, X. Zhou, J. Wang, N. Li, F. Liu, S. Gao, X. Liu, and W. Xu, "A radiomics nomogram for predicting the meningioma grade based on enhanced t 1wi images," *The British Journal of Radiology*, vol. 95, no. 1137, p. 20220141, 2022.

[56] A. Krizhevsky, I. Sutskever, and G. E. Hinton, "Imagenet classification with deep convolutional neural networks," *Communications of the ACM*, vol. 60, no. 6, pp. 84–90, 2017.

[57] K. Simonyan and A. Zisserman, "Very deep convolutional networks for large-scale image recognition," *arXiv preprint arXiv:1409.1556*, 2014.

[58] G. Zeng, Y. He, Z. Yu, X. Yang, R. Yang, and L. Zhang, "Going deeper with convolutions christian," in *Proc. IEEE Conf.*

Comput. Vis. Pattern Recognit.(CVPR), 2015, pp. 1–9.
[59] K. He, X. Zhang, S. Ren, and J. Sun, "Deep residual learning for image recognition," in *Proceedings of the IEEE conference on computer vision and pattern recognition*, 2016, pp. 770–778.
[60] A. Dosovitskiy, L. Beyer, A. Kolesnikov, D. Weissenborn, X. Zhai, T. Unterthiner, M. Dehghani, M. Minderer, G. Heigold, S. Gelly *et al.*, "An image is worth 16x16 words: Transformers for image recognition at scale," *arXiv preprint arXiv:2010.11929*, 2020.
[61] Z. Liu, Y. Lin, Y. Cao, H. Hu, Y. Wei, Z. Zhang, S. Lin, and B. Guo, "Swin transformer: Hierarchical vision transformer using shifted windows," in *Proceedings of the IEEE/CVF international conference on computer vision*, 2021, pp. 10 012–10 022.
[62] Z. Liu, H. Mao, C.-Y. Wu, C. Feichtenhofer, T. Darrell, and S. Xie, "A convnet for the 2020s," in *Proceedings of the IEEE/CVF conference on computer vision and pattern recognition*, 2022, pp. 11 976–11 986.
[63] Z. Lu, Y. Bai, Y. Chen, C. Su, S. Lu, T. Zhan, X. Hong, and S. Wang, "The classification of gliomas based on a pyramid dilated convolution resnet model," *Pattern Recognition Letters*, vol. 133, pp. 173–179, 2020.
[64] Y. Chen, Y. Lin, X. Xu, J. Ding, C. Li, Y. Zeng, W. Liu, W. Xie, and J. Huang, "Classification of lungs infected covid-19 images based on inception-resnet," *Computer methods and programs in biomedicine*, vol. 225, p. 107053, 2022.
[65] M. Abdar, M. A. Fahami, L. Rundo, P. Radeva, A. F. Frangi, U. R. Acharya, A. Khosravi, H.-K. Lam, A. Jung, and S. Nahavandi, "Hercules: Deep hierarchical attentive multilevel fusion model with uncertainty quantification for medical image classification," *IEEE Transactions on Industrial Informatics*, vol. 19, no. 1, pp. 274–285, 2022.
[66] J. Zhou, Z. Wu, Z. Jiang, K. Huang, K. Guo, and S. Zhao, "Background selection schema on deep learning-based classification of dermatological disease," *Computers in Biology and Medicine*, vol. 149, p. 105966, 2022.
[67] Q. Abbas, "An intelligent medical image classification system using few-shot learning," *Concurrency and Computation: Practice and Experience*, vol. 35, no. 2, p. e7451, 2023.
[68] J. Sun, B. Wu, T. Zhao, L. Gao, K. Xie, T. Lin, J. Sui, X. Li, X. Wu, and X. Ni, "Classification for thyroid nodule using vit with contrastive learning in ultrasound images," *Computers in Biology and Medicine*, vol. 152, p. 106444, 2023.
[69] L. Liu, H. Sun, and F. Li, "A lie group kernel learning method for medical image classification," *Pattern Recognition*, vol. 142, p. 109735, 2023.
[70] K. Cao, H. Tao, Z. Wang, and X. Jin, "Msm-vit: A multi-scale mobilevit for pulmonary nodule classification using ct images," *Journal of X-Ray Science and Technology*, no. Preprint, pp. 1–14, 2023.
[71] L. Yang, P. Xu, Y. Zhang, N. Cui, M. Wang, M. Peng, C. Gao, and T. Wang, "A deep learning radiomics model may help to improve the prediction performance of preoperative grading in meningioma," *Neuroradiology*, vol. 64, no. 7, pp. 1373–1382, 2022.
[72] A. Vassantachart, Y. Cao, M. Gribble, S. Guzman, J. C. Ye, K. Hurth, A. Mathew, G. Zada, Z. Fan, E. L. Chang *et al.*, "Automatic differentiation of grade i and ii meningiomas on magnetic resonance image using an asymmetric convolutional neural network," *Scientific Reports*, vol. 12, no. 1, p. 3806, 2022.
[73] W. Liu, T. Liu, T. Han, and L. Wan, "Multi-modal deep-fusion network for meningioma presurgical grading with integrative imaging and clinical data," *The Visual Computer*, vol. 39, no. 8, pp. 3561–3571, 2023.